

Regulation of axon growth *in vivo* by activity-based competition

Jackie Yuanyuan Hua^{1,2}, Matthew C. Smear³, Herwig Baier³ & Stephen J. Smith¹

¹Department of Molecular and Cellular Physiology, and ²Neurosciences Program, Stanford University, Stanford, California 94305, USA

³University of California, San Francisco, Department of Physiology, Program in Neuroscience, 1550 4th Street, San Francisco, California 94143-2722, USA

The formation of functional neural networks requires precise regulation of the growth and branching of the terminal arbors of axons, processes known to be influenced by early network electrical activity^{1–3}. Here we show that a rule of activity-based competition between neighbouring axons appears to govern the growth and branching of retinal ganglion cell (RGC) axon arbors in the developing optic tectum of zebrafish. Mosaic expression of an exogenous potassium channel or a dominant-negative SNARE protein was used to suppress electrical or neurosecretory activity in subsets of RGC axons. Imaging *in vivo* showed that these forms of activity suppression strongly inhibit both net growth and the formation of new branches by individually transfected RGC axon arbors. The inhibition is relieved when the activity of nearby ‘competing’ RGC axons is also suppressed. These results therefore identify a new form of activity-based competition rule that might be a key regulator of axon growth and branch initiation.

Pioneering studies of the development of mammalian peripheral motor axons have shown that axon arbor growth is governed by activity-based competition rules that appear to operate by means of an effect on branch elimination^{4,5}. Axon branches more active in releasing neurotransmitters persist at specific neuromuscular sites, whereas less active axon branches retract, resulting in the canonical elimination of polyneuronal innervation. There have been suggestions of analogous effects during the development of visual cortex^{6–8}, olfactory bulb^{9,10} and *Xenopus* optic tectum¹¹. Here we exploit the technically advantageous zebrafish optic tectum to test for a competition rule operating *in vivo* in a developing vertebrate brain. Previous work has firmly established a requirement of neural

activity in the refinement of the RGC tectal arbor and has identified some molecular pathways involved^{12–15}. We now report effects of suppressing activity in single RGC axons, with evidence for activity-based competition. Surprisingly, the competition effect in this case appears to be expressed primarily on the formation of new axon branches, rather than on branch stability.

Exogenous expression of the human inward rectifier K⁺ channel Kir2.1 has been shown to be a useful tool for electrically silencing individual neurons¹⁶. We used calcium imaging to test for the ability of Kir2.1 expression to suppress the excitability of zebrafish neurons. Figure 1a exemplifies the pattern of spontaneous and synchronized calcium spiking associated with spontaneous electrical activity in spinal cord neurons from larval zebrafish¹⁷. Figure 1b shows the effects of Kir2.1 expression on this calcium spiking. Whereas 41% of ventral lateral spinal neurons spiked in DsRed-expressing controls, only 6% ($P < 0.01$, binomial distribution statistics) spiked in those co-transfected with DsRed and Kir2.1. In animals expressing a non-conducting mutant version of Kir2.1 (Kirm)¹⁶, the percentage of active neurons was 50%, which was comparable to controls. These results indicate that Kir2.1 channel activity is effective in suppressing the electrical excitability of individual zebrafish neurons. Although optical imaging limitations precluded a direct test for silencing in transfected RGCs, it appears unlikely that effects of Kir2.1 in RGCs would be different from those observed in spinal cord neurons.

To express Kir2.1 in single RGCs, we isolated a 6-kilobase upstream sequence of the *brn3c* (*pou4f3*) gene (T. Xiao, T. Roeser, W. Staub and H. B., manuscript in preparation) as promoter. We chose zebrafish neuronal vesicle-associated membrane protein (VAMP) fused to green fluorescent protein (GFP) as an axon marker. Blastomere injection of *brn3c* promoter:GAL4 and a double UAS (the DNA recognition sequence that GAL4 binds to) cassette expressing Kir2.1 and VAMP-GFP led to just below 90% coexpression efficiency (Supplementary Fig. 1), which is consistent with an earlier report¹⁸. Most transfected animals expressed VAMP-GFP in a single RGC axon in one retina. We examined the effect of Kir2.1 expression on RGC axon arbor growth by measuring arbor length (as summed axon branch lengths) and complexity (as the number of branches per arbor) by two-photon microscopy *in vivo*. At 3 days after fertilization, when axons first start arborizing in the tectum, no differences were detected between

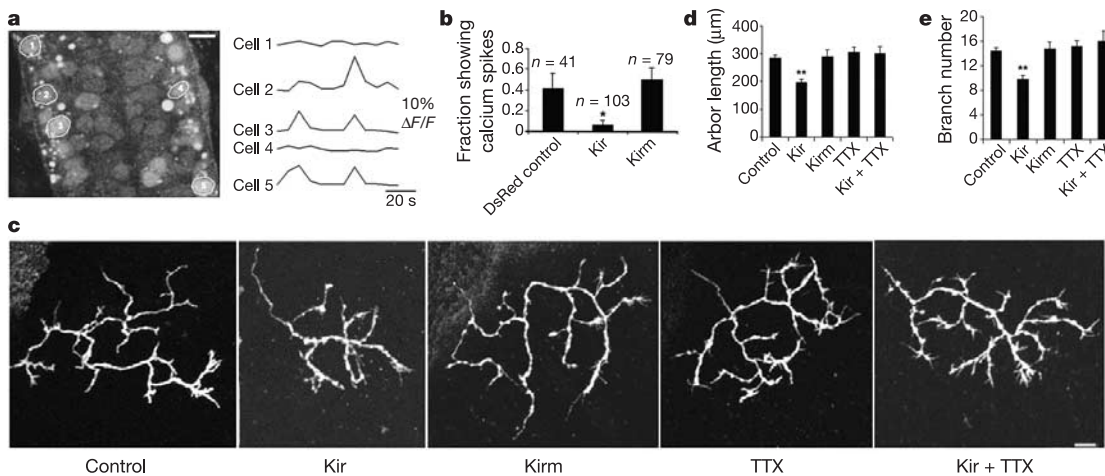


Figure 1 Kir2.1 overexpression inhibits zebrafish neuronal calcium spiking; expression in single RGCs inhibits axon arbor growth. **a**, Zebrafish ventral lateral spinal cord neurons exhibit spontaneous calcium spiking. The traces in the right panel show fluorescent intensity signals for the neurons marked by circles. The asterisk marks fluorescent cell debris. **b**, The fractions of neurons exhibiting calcium spiking ($n > 10$ animals for each

group). **c–e**, Sample axon arbor images (**c**), average axon arbor length (**d**) and branch number (**e**) for single transfected RGCs from animals at 5 days after fertilization. Control, $n = 34$; Kir, $n = 29$; Kirm, $n = 16$; TTX, $n = 19$; Kir + TTX, $n = 13$. Results are presented as means \pm s.e.m.; asterisk indicates $P < 0.01$, double asterisk indicates $P < 0.001$. Scale bar, 5 μ m.

Kir2.1-expressing (Kir) neurons and control neurons expressing only VAMP-GFP (data not shown). At 5 days after fertilization, however, Kir2.1 expression in single neurons caused a significant decrease in both arbor length (to 68% of control, $P < 0.001$) and arbor complexity (to 68% of control, $P < 0.001$) (Fig. 1c–e). In comparison, expression of the non-conducting Kir2.1 mutant (Kirm) had essentially no effect on either arbor length or complexity (Fig. 1c–e). It therefore seems that arbor growth inhibition by Kir2.1 is a result of Kir2.1 channel activity, acting through the suppression of electrical excitability.

The inhibition of axon growth by Kir2.1 channel activity could result directly from the suppression of RGC depolarization, or indirectly from blocking neurotransmitter release that is normally triggered by electrical excitation. To distinguish between these possibilities, we constructed a dominant-negative zebrafish VAMP-GFP protein (VAMPm) based on a mammalian dominant-negative VAMP mutant described previously¹⁹ (see Methods). Figure 2a, b shows results confirming the ability of VAMPm to block synaptic vesicle function with the use of the synaptic vesicle uptake marker FM1-43 (ref. 20). VAMPm overexpression suppresses vesicular FM1-43 uptake, reducing the fraction of

synaptic boutons exhibiting synaptic vesicle recycling in zebrafish motor neurons to 28% of control levels ($P < 0.001$).

VAMPm expression in single RGC axons did not affect arbor morphology at 3 days after fertilization (data not shown), but reduced axon arbor length and branch number to about 60% of control by 5 days after fertilization ($P < 0.001$, Fig. 2c–e). This growth inhibition is unlikely to be caused by VAMPm interference with SNARE proteins involved in intracellular trafficking, because SNARE interactions are pathway-specific *in vivo*²¹. Furthermore, VAMPm did not inhibit axon growth in conditions under which neural activity is globally blocked (see below). Because the inhibition of arbor growth by VAMPm resembles that caused by Kir2.1, most or all of the effects of electrical excitation might be due to depolarization-triggered neurotransmitter release.

To test for an activity-based competition rule, we measured the arbor growth of activity-suppressed cells when the activity of nearby cells was also suppressed in two different ways. We first performed imaging experiments in animals treated with an intraocular injection of tetrodotoxin (TTX) to block all RGC action potential firing. This TTX treatment did not affect the morphology of axons expressing VAMP-GFP, which is consistent with previous work¹⁴, but restored the growth of both Kir2.1-expressing (Fig. 1c–e) and VAMPm-expressing (Fig. 2c–e) RGC axon arbors to levels comparable ($P > 0.5$, that is, not significant) to the control. This

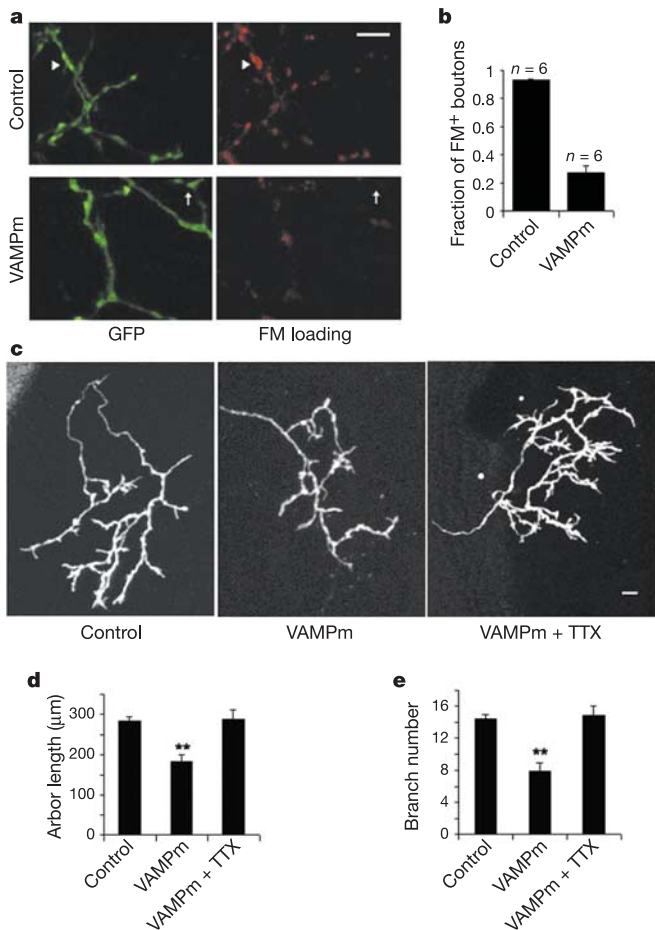


Figure 2 VAMPm overexpression suppresses presynaptic vesicle function in zebrafish neurons; expression in single RGCs inhibits axon arbor growth. **a, b**, Sample images (**a**) and quantification (**b**) of FM1-43 loading efficiency in VAMP-GFP (control) and VAMPm-expressing zebrafish spinal cord motor neurons. Arrowheads mark a FM1-43-loaded presynaptic bouton. Arrows mark a presynaptic bouton showing no FM1-43 uptake. $n = 6$ cells for each group. **c–e**, Sample axon arbor images (**c**), average axon arbor length (**d**) and branch number (**e**) for single transfected RGCs from animals at 5 days after fertilization. $n = 15$ for VAMPm, $n = 14$ for VAMPm + TTX. Results are presented as means \pm s.e.m.; double asterisk indicates $P < 0.001$. Scale bar, 5 μ m.

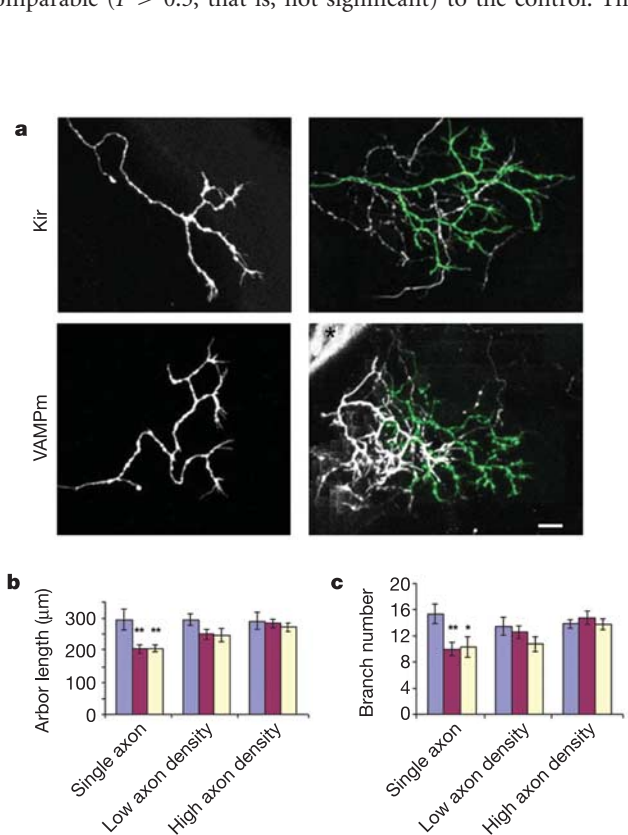


Figure 3 Transfection of multiple neighbouring RGC axons with Kir2.1 or VAMPm mitigates their growth-suppressing effects compared with transfection of a single axon. **a**, Sample images of electroporated RGCs at 5 days after fertilization. Single transfected axons are shown at the left, multiple transfected axons at the right. In each of the right panels one transfected axon arbor is highlighted in green. Skin fluorescence is marked by an asterisk. **b, c**, The axon arbor length (**b**) and branch number (**c**) for electroporated RGCs 5 days after fertilization. Axon densities between 0 and 0.095 μ m⁻¹ were classified as low, those between 0.095 and 0.19 μ m⁻¹ as high. Axon density was 0.089 for the highlighted Kir axon and 0.11 for the highlighted VAMPm axon in **a**. At least nine arbors were analysed for each condition. Colour coding in **b** and **c**: blue bars, control; maroon bars, Kir; yellow bars, VAMPm. Results are presented as means \pm s.e.m.; asterisk indicates $P < 0.01$, double asterisk indicates $P < 0.001$. Scale bar, 5 μ m.

pharmacological ‘rescue’ from the growth-inhibiting effects of single-cell activity inhibition indicates that competition from adjacent RGC axons, eliminated by the TTX treatment, might be responsible for the inhibition seen in the absence of TTX. However, TTX might diffuse from the eye into the brain and suppress activity in postsynaptic tectal cells, so it remains possible that an effect of direct competition between axons is distorted or obscured by silencing tectal cells with TTX.

In a second approach, which permitted a more selective suppression of activity in RGCs, we transfected groups of neighbouring RGCs by retinal electroporation. Sample images are shown in Fig. 3a. As expected if arbor growth is regulated by competition between neighbouring RGC axons, we observed a positive correlation between axon growth and the local density of axons expressing activity-suppressing constructs. To quantify the degree of overlap between transfected axons, each axon was assigned an ‘axon density’ value, based on the length of neighbouring transfected axon branches in its projection area. Figure 3b, c shows that growth inhibition was maximal in single transfected axons and returned almost to control levels at the highest axon densities achieved. The absence of an axon density effect for the control VAMP-GFP axons makes artificial effects of electroporation efficiency on axon growth unlikely. Comparisons with electron microscopic sections of tectal neuropil (S.J.S., unpublished data) and the stable *brn3c:mGFP* transgenic line (T. Xiao, T. Roeser, W. Staub and H.B., manuscript in preparation) indicate that even our highest densities of transfected axons might represent only a small fraction

of the axons converging into our imaging volumes. The axon density effect seen here indicates that the RGC subsets transfected by the retinal electroporation method might converge functionally in the tectum in some concerted way, predisposing them to strong growth competition.

Axon arbor growth is known to be a highly dynamic process: net arbor growth results from a balance between branch formation and elimination, with only a small fraction of new branches being maintained in the mature arbor²². To tease apart specific effects on arbor growth dynamics that underlie the activity-based competition, we collected time-lapse movies of single transfected RGC axons. Because the effects of competition on axon morphology are evident by 5 days after fertilization, we performed time-lapse imaging at 4–5 days after fertilization (100–112 h after fertilization).

We collected images at 2-min intervals for 40–50 min to capture rapid axon dynamics (Fig. 4a and Supplementary Movies 1–3). Expression of VAMPm and Kir2.1 in single RGCs substantially suppressed arbor motility (scored by summing the absolute values of length changes across all branches and time points) (Fig. 4b; Kir2.1 39% of control, VAMPm 59% of control, $P < 0.001$), and branch formation rates (Fig. 4c; Kir2.1 45% of control, VAMPm 56% of control, $P < 0.001$). About 95% of the newly formed branches were present in more than one image in the time-lapse sequences; the reduced branch formation rates observed were therefore unlikely to have been due to shortening of transient branch lifetimes to below detection.

In contrast, Kir2.1 and VAMPm expression in single RGCs did

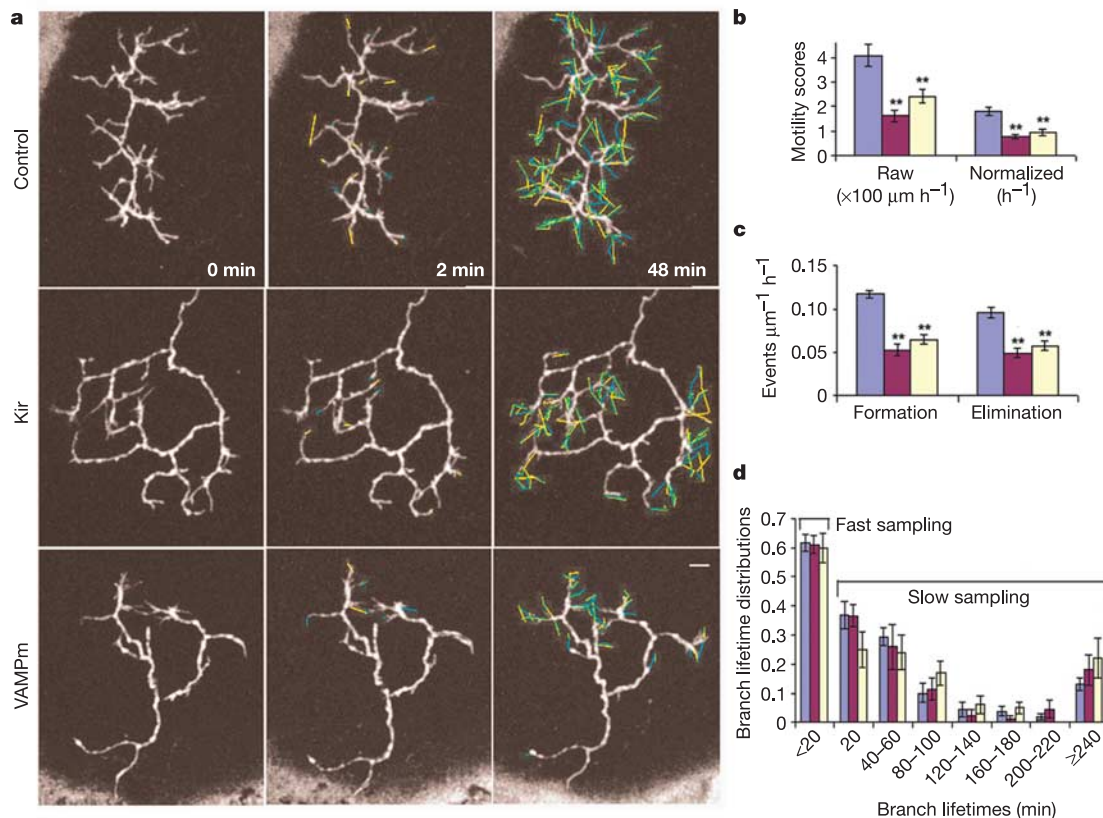


Figure 4 Selective activity suppression inhibits axon motility and branch formation rate with little effect on branch stability. **a**, Sample images taken from 2-min interval (fast-sampling) movies. The branch end positions between consecutive time points were connected by lines colour-coded for length change: yellow for increase, cyan for decrease. Traces in which branch extension and retraction overlap appear green. The middle panels show branch end position changes in the first 2 min; the right panels show the cumulative changes in 48 min. **b**, Motility scores from fast-sampling movies before

and after normalization to initial axon arbor length. $n = 9$ for control; $n = 8$ for Kir2.1 and VAMPm. **c**, Branch formation rates and elimination rates determined from fast-sampling movies. **d**, Lifetime distribution of newly formed branches for fast-sampling and slow-sampling (20-min interval) movies. At least 104 branches were analysed for each group. Colour coding in **b–d**: blue bars, control; maroon bars, Kir; yellow bars, VAMPm. Results are presented as means \pm s.e.m.; double asterisk indicates $P < 0.001$. Scale bar, 5 μ m.

not affect axon branch stability. Of the new branches that formed at least 20 min before the end of imaging, similar proportions were eliminated within 20 min in control ($62 \pm 3\%$), Kir2.1 ($61 \pm 3\%$) and VAMPm ($60 \pm 5\%$) neurons. We also imaged axons at 20-min intervals for 8 h (Supplementary Movies 4–6) to determine branch stability over a longer time course. The lifetime distribution of branches formed during the first 4 h of imaging showed no statistical difference between control, Kir and VAMPm neurons (Fig. 4d), confirming a lack of activity-suppression effect on branch stability. Although Kir2.1 and VAMPm expression produced large reductions in branch elimination rates (Fig. 4c), the lack of any obvious competition effect on branch lifetime indicates that the reduced elimination rates might have been simply a consequence of the reductions in branch formation rates (that is, fewer transient branches were eliminated because fewer new branches formed).

Most of the cellular mechanisms at the heart of the competition rule we described here remain unknown. However, our results do indicate that many or all of the competition effects might be mediated by VAMP-dependent synaptic vesicle function. It is possible that some other consequence of synaptic vesicle function, such as co-transmitter release or membrane turnover, is involved, but it seems most likely that the released neurotransmitter itself mediates the observed effect, binding to nearby axon arbors or else to postsynaptic tectal cells or glial cells that feed back onto the RGC arbors through retrograde signals. Several plausible candidates for such a retrograde signal have been proposed, including neurotrophins, nitric oxide and arachidonic acid^{13,23,24}.

Discerning simple developmental rules that govern the construction of complex neural circuits is a central aspiration of developmental neuroscience. Here we present evidence for a specific competition rule in which the growth of an axon arbor is inhibited when its activity is suppressed below that of active neighbours. Our high-resolution time-lapse data further indicate that under the conditions examined such competition might govern the formation of new axonal branches but not branch stability. Compared with competition rules governing branch stabilization alone, competitive regulation of branch formation might increase the efficiency with which a dynamic axon arbor could 'explore' large neuropil volumes for appropriate synaptic partners. □

Methods

Ethical approval

All experimental protocols were approved by the Stanford University Animal Care and Use Committee.

Vector production

The *brn3c*:GAL4 vector was based on PB-GAL4VP16 (a gift from S. E. Fraser). In zebrafish neuronal VAMP-GFP (a gift from J. D. Jontes), GFP was tagged to the carboxyl terminus of VAMP. VAMP-GFP recycles between synaptic vesicles and the cell membrane, so it distributes in both a punctate and a membrane-targeted pattern, strongly labelling axon branch tips. To generate VAMPm, mutations of VAMP E81A, S82A were introduced to VAMP-GFP by polymerase chain reaction. Human Kir2.1 and the non-conducting mutant, in which the pore-region amino-acid motif GYG was mutated to AAA, were gifts from V. N. Murthy and E. Marban. A Myc tag was added to the amino terminus of Kir2.1 by polymerase chain reaction. UAS:VAMP-GFP:pA was inserted before the UAS sequence of UAS:Kir2.1:pA so that RNA transcription proceeded in the same direction. pA refers to the polyadenylation signal from Clontech PEGFP-N1 as a *NotI/AflII* fragment. The pA following VAMP-GFP was inverted during subcloning, inverting the two original AATAAA motifs and creating a new one. Double UAS constructs and *brn3c* promoter:GAL4 were linearized for injection.

Embryo maintenance

Embryos were raised in the dark at 28 °C in the presence of 150 μM 1-phenyl-2-thiourea to prevent pigment formation. The RGC axon morphology of animals raised in the dark was comparable to that of animals raised on a 14 h:10 h light–dark cycle at 5 days after fertilization (axon arbor length 295 ± 23 μm, branch number 13.7 ± 1.5 , $n = 16$). For TTX treatment, larvae received an intraocular injection of 8–10 nl of 0.6 mM TTX (Calbiochem) in Ringer solution. Injection at 2 or 3 days after fertilization led to similar effects on RGC axon development, and the data were pooled for analysis.

RGC axon imaging and data analysis

Zebrafish larvae were immobilized in agarose. Z-series stacks were collected at 1.5-μm intervals. Because RGC axons arborizing in the anterior tectum tend to have small projection areas and short arbor lengths, only axons arborizing in the posterior two-thirds of the tectum were considered. Axons with a GFP intensity higher than double the auto-fluorescence of skin were excluded from analysis. VAMP-GFP expression at the levels used here did not affect axon morphology compared with axons expressing GFP (axon arbor length $2,875 \pm 24$ μm, branch number 14.6 ± 0.9 , $n = 10$). For time-lapse analysis, axons transfected by blastomere injection with axon arbor lengths of 200–300 μm were chosen. For image analysis, processes at least 2 μm long were considered branches. Growth cones bearing multiple filopodia were considered single branches. Axons at 5 days after fertilization were reconstructed three-dimensionally. For time-lapse analysis, maximum-intensity projections were used. The Kolmogorov–Smirnov test was used for statistics unless otherwise noted.

Calcium green-1 imaging

Calcium green-1 dextran (10 mM; 10 kDa; Molecular Probes) was injected into embryos together with α-tubulin promoter:GAL4 and UAS:DsRed or DsRed, Kir2.1 double-UAS construct. Larvae at 24–27 h after fertilization were immobilized in 100 μg ml⁻¹ curare for imaging. Images were collected from the ventral spinal cord (within 20 μm from the notochord) at 10-s intervals for 2 min. (Optical artefacts due to lens and pigment precluded effective calcium imaging from RGC cell bodies in the retina. No method tried permitted the imaging of useful calcium signals from RGC axons.) Images were analysed with Openview software (authored by N. Ziv, Technion, Haifa, Israel). Ventral lateral spinal cord neurons showing 10% or more increases in fluorescent intensity in cell bodies were considered to be spiking. Neurons that fired at least once during the imaging interval were scored as active.

FM1-43 loading assay

FM1-43 loading was performed in zebrafish larvae 3 days after fertilization as described in ref. 20, except that the FM1-43 preloading incubation was omitted and the incubation in Advasep-7 after loading was extended to 15 min. For data analysis, regions of the motor neuron axons with a GFP intensity higher than double the intensity of shaft region were considered presynaptic boutons. FM1-43 puncta with an intensity of 80–255 and a size of 0.5–2 μm were considered synaptic.

Retinal electroporation

Electroporation was performed as described in ref. 25. DNA plasmids were injected into the intraocular space of larvae at 2 days after fertilization. Three or four square 15-ms current pulses of 0.3 mA were delivered at 1-s intervals between a fine wire electrode placed near the injected eye and a distant ground electrode. Arbor length and branch number were measured from three-dimensional images. To measure axon density, Z-series stacks consisted of minimal numbers of sections containing the axon arbors of interest. Neighbouring transfected axon branches contained within this Z stack and the projection area of the arbor of interest were traced. Their summed length divided by the projection area produced the axon density value for the arbor of interest.

Received 21 April 2004; accepted 28 January 2005; doi:10.1038/nature03409.

- Sanes, J. R. & Lichtman, J. W. Development of the vertebrate neuromuscular junction. *Annu. Rev. Neurosci.* **22**, 389–442 (1999).
- Katz, L. C. & Shatz, C. J. Synaptic activity and the construction of cortical circuits. *Science* **274**, 1133–1138 (1996).
- Zhang, L. I. & Poo, M. M. Electrical activity and development of neural circuits. *Nature Neurosci.* **4** (Suppl), 1207–1214 (2001).
- Buffelli, M. *et al.* Genetic evidence that relative synaptic efficacy biases the outcome of synaptic competition. *Nature* **424**, 430–434 (2003).
- Lichtman, J. W. & Balice-Gordon, R. J. Understanding synaptic competition in theory and in practice. *J. Neurobiol.* **21**, 99–106 (1990).
- Shatz, C. J. & Stryker, M. P. Ocular dominance in layer IV of the cat's visual cortex and the effects of monocular deprivation. *J. Physiol. (Lond.)* **281**, 267–283 (1978).
- Stryker, M. P. & Harris, W. A. Binocular impulse blockade prevents the formation of ocular dominance columns in cat visual cortex. *J. Neurosci.* **6**, 2117–2133 (1986).
- Antonini, A. & Stryker, M. P. Rapid remodeling of axonal arbors in the visual cortex. *Science* **260**, 1819–1821 (1993).
- Yu, C. R. *et al.* Spontaneous neural activity is required for the establishment and maintenance of the olfactory sensory map. *Neuron* **42**, 553–566 (2004).
- Zhao, H. & Reed, R. X. Inactivation of the *OCN1* channel gene reveals a role for activity-dependent competition in the olfactory system. *Cell* **104**, 651–660 (2001).
- Ruthazer, E. S., Akerman, C. J. & Cline, H. T. Control of axon branch dynamics by correlated activity *in vivo*. *Science* **301**, 66–70 (2003).
- Schmidt, J. T., Buzzard, M., Borress, R. & Dhillon, S. MK801 increases retinotectal arbor size in developing zebrafish without affecting kinetics of branch elimination and addition. *J. Neurobiol.* **42**, 303–314 (2000).
- Schmidt, J. T., Fleming, M. R. & Leu, B. Presynaptic protein kinase C controls maturation and branch dynamics of developing retinotectal arbors: possible role in activity-driven sharpening. *J. Neurobiol.* **58**, 328–340 (2004).
- Gnueghe, L., Schmid, S. & Neuhaus, S. C. Analysis of the activity-deprived zebrafish mutant *macho* reveals an essential requirement of neuronal activity for the development of a fine-grained visuotopic map. *J. Neurosci.* **21**, 3542–3548 (2001).
- Johnson, F. A., Dawson, A. J. & Meyer, R. L. Activity-dependent refinement in the goldfish retinotectal system is mediated by the dynamic regulation of processes withdrawal: an *in vivo* imaging study. *J. Comp. Neurol.* **406**, 548–562 (1999).
- Burrone, J., O'Byrne, M. & Murthy, V. N. Multiple forms of synaptic plasticity triggered by selective suppression of activity in individual neurons. *Nature* **420**, 414–418 (2002).

17. Drapeau, P. *et al.* Development of the locomotor network in zebrafish. *Prog. Neurobiol.* **68**, 85–111 (2002).
18. Koster, R. W. & Fraser, S. E. Tracing transgene expression in living zebrafish embryos. *Dev. Biol.* **233**, 329–346 (2001).
19. Sorensen, J. B. *et al.* The SNARE protein SNAP-25 is linked to fast calcium triggering of exocytosis. *Proc. Natl Acad. Sci. USA* **99**, 1627–1632 (2002).
20. Li, W., Ono, F. & Brehm, P. Optical measurements of presynaptic release in mutant zebrafish lacking postsynaptic receptors. *J. Neurosci.* **23**, 10467–10474 (2003).
21. Scales, S. J. *et al.* SNAREs contribute to the specificity of membrane fusion. *Neuron* **26**, 457–464 (2000).
22. Hua, J. Y. & Smith, S. J. Neural activity and the dynamics of central nervous system development. *Nature Neurosci.* **7**, 327–332 (2004).
23. Cogen, J. & Cohen-Cory, S. Nitric oxide modulates retinal ganglion cell axon arbor remodeling *in vivo*. *J. Neurobiol.* **45**, 120–133 (2000).
24. Cohen-Cory, S. & Fraser, S. E. Effects of brain-derived neurotrophic factor on optic axon branching and remodelling *in vivo*. *Nature* **378**, 192–196 (1995).
25. Haas, K., Jensen, K., Sin, W. C., Foa, L. & Cline, H. T. Targeted electroporation in *Xenopus* tadpoles *in vivo*—from single cells to the entire brain. *Differentiation* **70**, 148–154 (2002).

Supplementary Information accompanies the paper on www.nature.com/nature.

Acknowledgements We thank T. R. Clandinin, R. W. Tsien, R. W. Aldrich, L. Luo and the Smith laboratory for comments on the manuscript, and C. M. Niell for developing the Matlab routines used in image analysis. We thank T. Roeser for isolating the *brn3c* promoter. The US National Institutes of Health and the Vincent Coates Foundation provided financial support. J.Y.H. was supported by a Stanford Graduate Fellowship and a Coates Foundation Fellowship. M.C.S. was supported by a predoctoral fellowship from the American Heart Association.

Competing interests statement The authors declare that they have no competing financial interests.

Correspondence and requests for materials should be addressed to J.Y.H. (huay@stanford.edu).

Hypothalamic K_{ATP} channels control hepatic glucose production

Alessandro Pocai¹, Tony K. T. Lam¹, Roger Gutierrez-Juarez¹, Silvana Obici¹, Gary J. Schwartz¹, Joseph Bryan², Lydia Aguilar-Bryan² & Luciano Rossetti¹

¹Departments of Medicine, Neuroscience and Molecular Pharmacology, Diabetes Research Center, Albert Einstein College of Medicine, Bronx, New York 10461, USA

²Department of Medicine, Baylor College of Medicine, Houston, Texas 77030, USA

Obesity is the driving force behind the worldwide increase in the prevalence of type 2 diabetes mellitus^{1,2}. Hyperglycaemia is a hallmark of diabetes and is largely due to increased hepatic gluconeogenesis³. The medial hypothalamus is a major integrator of nutritional and hormonal signals^{1,2,4}, which play pivotal roles not only in the regulation of energy balance but also in the modulation of liver glucose output^{5,6}. Bidirectional changes in hypothalamic insulin signalling therefore result in parallel changes in both energy balance^{7–10} and glucose metabolism⁵. Here we show that activation of ATP-sensitive potassium (K_{ATP}) channels¹¹ in the mediobasal hypothalamus is sufficient to lower blood glucose levels through inhibition of hepatic gluconeogenesis. Finally, the infusion of a K_{ATP} blocker within the mediobasal hypothalamus, or the surgical resection of the hepatic branch of the vagus nerve, negates the effects of central insulin and halves the effects of systemic insulin on hepatic glucose production. Consistent with these results, mice lacking the SUR1 subunit of the K_{ATP} channel¹² are resistant to the inhibitory action of insulin on gluconeogenesis. These findings suggest that activation of hypothalamic K_{ATP} channels normally restrains hepatic gluconeogenesis, and that any alteration

within this central nervous system/liver circuit can contribute to diabetic hyperglycaemia.

ATP-sensitive potassium (K_{ATP}) channels are expressed in the hypothalamus¹³ and can be activated by insulin (and leptin) in selective hypothalamic neurons^{14,15}. However, the functional role of insulin activation of hypothalamic K_{ATP} channels remains obscure. To investigate whether direct activation of central K_{ATP} channels is sufficient to reproduce the potent effects of insulin on blood glucose levels, on glucose production, and on hepatic gluconeogenesis, we infused the K_{ATP} channel activator diazoxide in the third cerebral ventricle (ICV) of conscious rats. Central administration of diazoxide lowered blood glucose levels (Fig. 1a). To examine the mechanisms by which central activation of K_{ATP} channels decreases blood glucose, we combined ICV infusions of vehicle or diazoxide with systemic pancreatic insulin-clamp studies (Supplementary Fig. S1a). In the presence of basal circulating insulin levels (~20 μU ml⁻¹), glucose infusion was required to prevent hypoglycaemia following central administration of diazoxide (Fig. 1b). We next assessed glucose kinetics to establish whether the increased requirement for glucose infusion in response to central activation of K_{ATP} channels is due to stimulation of glucose uptake or to inhibition of glucose production. ICV diazoxide markedly and significantly decreased glucose production (by 45 ± 4%; Fig. 1b), but the rate of glucose uptake was not significantly affected (Supplementary Fig. S1b). Thus, central stimulation of K_{ATP} channels lowers blood glucose by inhibiting glucose production.

Glucose production represents the net increase in glucosyl units derived from gluconeogenesis and glycogenolysis. However, a portion of glucose entering the liver as a result of glucose phosphorylation is also a substrate for dephosphorylation by glucose-6-phosphatase (G6Pase), creating a futile cycle of glucose cycling (Supplementary Fig. S1a). In order to further delineate the mechanisms by which central activation of K_{ATP} channels modulates glucose homeostasis, we estimated the *in vivo* flux through G6Pase and the relative contribution of gluconeogenesis and glycogenolysis to glucose output. ICV diazoxide infusion decreased the flux through G6Pase (Supplementary Fig. S1c) in parallel with its effects on glucose production (Fig. 1b). Importantly, the decrease in glucose production was largely accounted for by marked inhibition of gluconeogenesis (Fig. 1b), while the rate of glycogenolysis was not significantly decreased (Supplementary Fig. S1d). Real-time polymerase chain reaction (PCR) analysis showed that ICV diazoxide infusion markedly decreased messenger RNA levels of liver *G6Pase* (also known as *G6pc* in mouse and rat) and of the gluconeogenic gene *Pepck* (*phosphoenolpyruvate kinase*, also known as *Pck1* in mouse and rat) (Fig. 1c). Thus, direct activation of central K_{ATP} channels was sufficient to mimic the actions of insulin on gluconeogenesis, the *in vivo* fluxes through G6Pase, and the hepatic expression of *G6Pase* and *Pepck*.

The potent metabolic effects of diazoxide could be mediated by its activation of K_{ATP} channels anywhere within the central nervous system (CNS)¹⁶. To examine the anatomical localization of these effects we infused a 15-fold lower dose of diazoxide (Fig. 1e) bilaterally within the parenchyma of the medial hypothalamus (Supplementary Fig. S2a). Intrahypothalamic infusion of diazoxide lowered blood glucose levels (Fig. 1d). This hypoglycaemic effect was due to marked suppression of glucose production (Fig. 1d). To examine whether the effects of ICV insulin on liver glucose homeostasis⁵ are also centred in an overlapping hypothalamic area, we next performed intrahypothalamic infusions of insulin (Fig. 1e) at a dose 15-fold lower than that previously used in ICV experiments⁵. Intrahypothalamic insulin reproduced the potent effects of ICV insulin on blood glucose concentration and on glucose infusion and gluconeogenesis (Fig. 1e). Thus, activation of either K_{ATP} channels or of insulin signalling within the medial hypothalamus is sufficient to decrease blood glucose levels through